CAMBRIDGE
UNIVERSITY PRESS

Article

Hierarchical layered double hydroxide for the removal of charged dyes: the role of an anionic surfactant

Xuefen Zhang[1], Mingxue Xiang[2], Zhongbang Zhu[2], Youqin Zou[2] and Ping Zhang[2]*

[1]State Key Laboratory of Nuclear Resources and Environment, East China University of Technology, Nanchang 330031, China and [2]Key Laboratory of Poyang Lake Environment and Resource Utilization, Ministry of Education, School of Environmental and Chemical Engineering, Nanchang University, Nanchang 330031, China

Abstract

Hierarchical layered double hydroxide (HLDH) was synthesized by using sodium dodecyl sulfate (SDS) as a soft-template agent for the removal of two charged organic dyes (i.e. methylene blue (MB; cationic dye) and methyl orange (MO; anionic dye)). The experimental results based on response surface methodology (RSM) demonstrated distinct removal behaviours of HLDH towards these two dyes: (1) the maximum capacity was 416.7 mg g^{-1} for MO and 58.7 mg g^{-1} for MB at 25°C; (2) the increase in temperature could enhance MO removal significantly, whereas it had a negligible effect on the MB treatment process; and (3) rapid removal of MB (5 min) compared to MO (480 min) was observed. In addition, the removal process for both dyes was pH-independent. Multiple characterization techniques further revealed the removal mechanisms, demonstrating that SDS played a significant role in the removal of both dyes; that is, MO replaced SDS to be intercalated into the HLDH interlayer *via* anion exchange. MB could influence the –SO$_3$ group of SDS, resulting in it modifying the electrodensity of SDS. It could then be further combined with an SDS anion (DS$^-$) *via* hydrophobic and electrostatic interactions to form DS-MB monolayers. This work not only provides an efficient capture agent for charged dyes, but also offers a deep insight into the underlying removal mechanism.

Since the turn of the twentieth century, clay minerals have been research tools for scientists due to their multiple intriguing properties (e.g. charged surface, molecular sieve structure and ion exchange character; Weber *et al.*, 2014; Arif *et al.*, 2021). Layered double hydroxides (LDHs), with their two-dimensional (2D) sandwich-structure composed of a positively charged metal hydroxide host layer together with charge-balancing anions and water in the interlayer, are among the most common anionic clay minerals (Ma *et al.*, 2016; Suh *et al.*, 2020). Due to their unique structure, the LDHs exhibit excellent properties, such as a tuneable composition, a high dispersion of cations and a large specific surface area, which endow LDHs with superior performance in photocatalysis, electrocatalysis and supercapacitors (Abderrazek *et al.*, 2015; Gao *et al.*, 2016; Hong *et al.*, 2019; Jing *et al.*, 2019). Remarkably, LDHs have another prominent feature (i.e. 'anion-exchange capacity') that permits external anionic species in the solution to be inserted into the interlayer regions of the LDHs (Yang *et al.*, 2004; de Castro *et al.*, 2018). In view of these characteristics, the Fe$_3$O$_4$/MgAl-LDH has achieved high adsorption capacity for Congo red (253 mg g^{-1}; Shan *et al.*, 2014), and NiFe-LDH was used to remove methyl orange (MO) from water with a maximum adsorption of 323.6 mg g^{-1} (Hu

et al., 2020). Obviously, LDHs may serve as potential water purification agents for removal of anionic pollutants.

Recently, interest in LDHs has focused on tuning the 2D structure to a three-dimensional (3D) structure to enhance their adsorption capacity (Li & He, 2008; Jiehu *et al.*, 2020). In this context, hierarchical LDHs with 3D structures have been designed with greater specific surface areas and pore volumes than those of 2D LDHs (Sun *et al.*, 2015; Zheng *et al.*, 2019). A novel hierarchically porous Fe$_3$O$_4$@MgAl-LDH was produced and used to eliminate Congo red, which exhibited superb adsorption capacity (813.0 mg g^{-1}) compared with pure MgAl-LDH (Lu *et al.*, 2017). Miao *et al.* (2021) prepared a hollow hierarchical porous CoMgAl-borate LDH for MO elimination with an extraordinary adsorption capacity of 990.1 mg g^{-1}. In our previous work, we had successfully prepared an organic hierarchical LDH (HLDH) *via* a soft-template method using sodium dodecyl sulfate (SDS) as a template agent and intercalated anions (Zhang *et al.*, 2019a). Interestingly, the SDS introduced not only changed the positive surface charge of the LDH to negative, but also rendered the surface hydrophobic (Bayram *et al.*, 2020). Numerous reports reveal that such an evolution is favourable for cationic pollutant removal with adsorbents (Lin *et al.*, 2018; Liu *et al.*, 2021; Romero Ortiz *et al.*, 2021). Few comprehensive reports exist, however, on the utilization of HLDHs to remove various charged organics, or which focus on the underlying mechanisms.

In view of the fact that wastewaters contain numerous charged pollutants, an organic HLDH intercalated with SDS was employed here for the removal of two charged organic pollutants, namely

methylene blue (MB; a cationic heteroaromatic compound) and MO (an anionic azo dye). Moreover, the response surface methodology (RSM), a powerful statistical technique to optimize the reaction parameters as well as to explore their interactions, was employed to reveal the adsorption performance based on central composite design (CCD) (Igwegbe *et al.*, 2019; Yuan *et al.*, 2020). The interaction mechanisms of the two variously charged dyes with the HLDH were further investigated *via* thermal analysis, Fourier-transform infrared (FTIR) spectroscopy, X-ray photoelectron spectroscopy (XPS), X-ray powder diffraction (XRD) and scanning electron microscopy (SEM). The results are expected to open up a new avenue for charged pollutant removal and to broaden the application of anionic clay minerals in water purification.

Experimental

Materials

$Mg(NO_3)_2 \cdot 6H_2O$, $Al(NO_3)_3 \cdot 9H2O$, urea (CH_4N_2O), SDS, MB and MO of analytical grade were purchased from Aladdin and used without further purification. The physicochemical properties of the organics are shown in Table S1. Deionized water was used in all of the experiments.

Materials preparation

The HLDH was synthesized *via* a soft-template method (Zhang *et al.*, 2019b), with a molar ratio of Mg:Al:urea of 2:1:10 dissolved in 50 mL of deionized water (Solution A). Separately, 0.865 g SDS was dissolved in 30 mL of deionized water (Solution B). Thereafter, Solution B was immediately added to Solution A under stirring and was sonicated for 30 min. The homogeneous solution was transferred into a 100 mL Teflon-lined autoclave and heated at 150°C for 6 h. After air-cooling, the product was centrifuged, washed four times with water and ethanol and dried at 65°C overnight.

Batch experiment

Sorption isotherm experiments for MB and MO were carried out based on the RSM as described in the next section. A kinetic study was performed with an initial concentration of MB/MO of 100 mg/L at 25°C. The effect of solution pH was investigated within the pH range 3–11 adjusted by 1 M HCl and NaOH. The dosage of HLDH in all tests was 1.0 g L^{-1}. The mixtures were stirred for 12 h at 150 rpm. After filtration through 0.45 μm membrane filters, the equilibrium concentrations of MB and MO were measured using an ultraviolet–visible spectrophotometer (UV-1600 spectrophotometer) at maximum absorbance wavelengths of 664 and 464 nm, respectively.

The adsorption of MB and MO on HLDH was determined using Eq. 1:

$$q_e = \frac{(C_0 - C_e)V}{m} \qquad (1)$$

where q_e (mg g^{-1}) is the adsorption of MB and MO at equilibrium, V (L) is the volume of the MB and MO solution, C_0 and C_e (mg L^{-1}) are the initial and equilibrium concentrations of MB and MO, respectively, and m (g) is the mass of HLDH.

Table 1. Independent factors of MB and their levels used in the CCD model.

Variable	Unit	Factor	−α	−1	0	+1	+α
Temperature	°C	X_1	20.8579	25	35	45	49.142
Concentration	g L^{-1}	X_2	18.9341	50	125	200	231.066

Table 2. Independent factors of MO and their levels used in the CCD model.

Variable	Unit	Factor	−α	−1	0	+1	+α
Temperature	°C	X_1	20.8579	25	35	45	49.142
Concentration	g L^{-1}	X_2	20.5887	120	360	600	699.411

Central composite design-based RSM

A two-factor and one-level CCD model was constructed to investigate the removal behaviour of MO and MB on HLDH. The coding limits and levels of selected variables (i.e. temperature and initial concentration) are listed in Tables 1 and 2, respectively. The actual experimental parameters are listed in Tables S2 and S3. The experimental data were evaluated using *Design-Expert* (8.0.6, trial version) software. Additionally, the accuracy of the CCD model was determined using analysis of variance (ANOVA) to avoid poor or ambiguous results, as is shown in Tables S4 and S5. The detailed analyses are shown in the Supplementary Information.

Preparation of HLDH_MB and HLDH_MO

For the synthesis of HLDH_MB, HLDH (1 g L^{-1}) was added to 200 mg L^{-1} MB solution. The mixture was stirred at 150 rpm for 12 h. Subsequently, the solid phase was separated by filtration and dried at 65°C for 12 h. HLDH_MO was synthesized using a similar method, except for the initial MO concentration (1000 mg L^{-1}).

Characterization of the end products

The FTIR spectra were obtained using a Bruker Tensor 27 spectrometer in the 4000–400 cm^{-1} range. Surface elemental compositions were identified using XPS (Kratos Axis ULTRA X-ray photoelectron spectrometer). Powder XRD was conducted using a D8 ADVANCE X diffractometer with Cu-$K\alpha$ radiation (40 kV, 100 mA) at a scan speed of 4°2θ min^{-1} in the range 2–65°2θ. Scanning electron microscopy (JSM 6701F) was used to observe the morphology of the samples. Thermogravimetry and differential thermal analysis (TG-DTA) were performed using the NETZSCH simultaneous TG-DTA/differential scanning calorimetry (DSC) apparatus STA 449C/4/G Jupiter-QMS 403C Aeolos in the range 40–1000°C at a heating rate of 10°C min^{-1} in a pure N_2 atmosphere. The pH values were monitored using an Elico digital pH meter (Model LI-120).

Results and discussion

Adsorption behaviour of MO and MB

The adsorption performance of HLDH towards MB and MO with various initial concentrations and temperatures was investigated
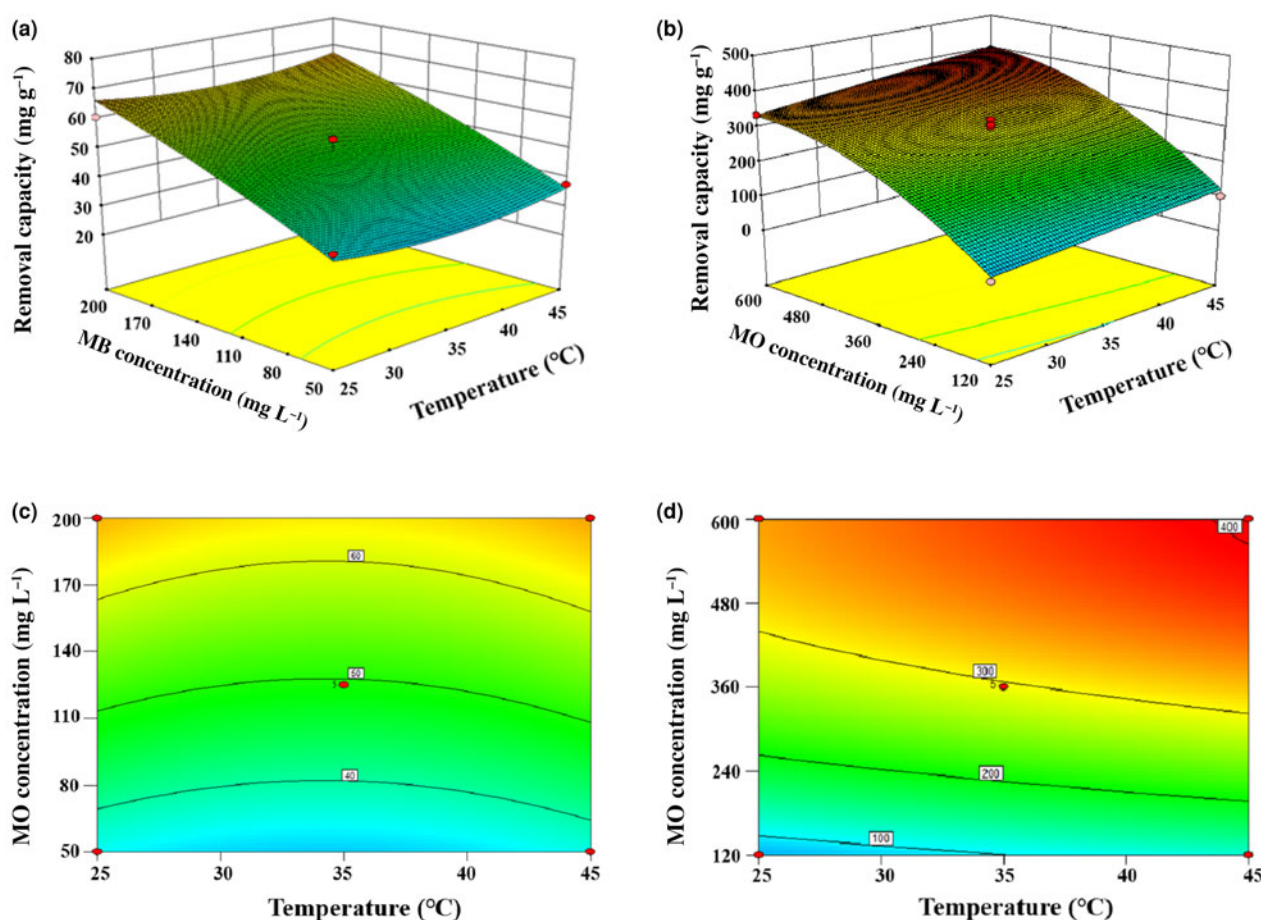
Fig. 1. Adsorption capacities of (a, c) MB and (b, d) MO by the HLDH *via* the RSM. Conditions: adsorbent dosage for MB/MO = 1 g L^{-1}; contact time = 12 h.

using the RSM. The 2D contour plots and 3D response surfaces obtained are shown in Fig. 1. The adsorption of MB was maximal at high initial MB concentrations, but the amount of dye removed did not change as the temperature increased from 25°C to 45°C (Fig. 1a,c). In the case of MO, the amount removed was also maximal at high initial MO concentrations, but it increased with increasing temperature (Fig. 1b). The influence of the initial MO concentration on MO adsorption was greater than the influence of MB. Indeed, the density contour obtained for the initial MO concentration in the RSM was more pronounced than that of temperature (Fig. 1d). Both results demonstrated a more significant effect of the initial concentration on the MO adsorption, implying different removal pathways for MB and MO by HLDH (Zhang *et al.*, 2019b). Notably, the maximum adsorption capacities of MB and MO on HLDH at 25°C were 58.7 and 416.7 mg g^{-1}, respectively, which are superior to those of the other adsorbents (Table S6).

To evaluate the effectiveness of the HLDH for absorbing both dyes, kinetic experiments were performed at an initial MB/MO concentration of 100 mg L^{-1} (Fig. 2). The adsorption of MB rapidly reached equilibrium within 5 min, with the maximum adsorption being 44.4 mg g^{-1}. In the case of MO, the adsorption was rapid in the first 60 min, and then gradually reached a plateau at 480 min (64.1 mg g^{-1}). The rapid removal of MB compared to MO further illustrates the existence of different interaction mechanisms for the two charged dyes on HLDH.

The effect of pH on the removal of MB and MO by HLDH is exhibited in Fig. 3. The adsorption of both dyes varied slightly over the pH range 3–9 and decreased at pH 11. This reduced adsorption amount might be associated with the unstable structure of LDHs in strong alkali environments (Xu *et al.*, 2008).

In addition, the ζ-potential of the HLDH was examined to explore the reaction pathway. The ζ-potential remained negative across the whole pH range, suggesting a negative surface charge for the HLDH (Fig. S1). Given that MB and MO are cationic and anionic dyes in solution, respectively, it is reasonable to deduce that electrostatic attraction contributed to MB removal by HLDH, whereas electrostatic repulsion occurred in MO removal. However, the adsorption of MO (61.0 mg g^{-1}) was superior to that of MB (40.9 mg g^{-1}), suggesting that electrostatic interaction was not the only mechanism controlling the reaction process.
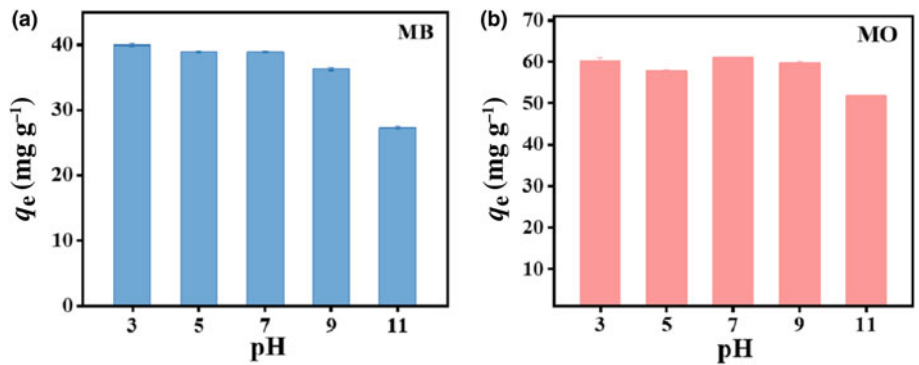
Adsorption isotherms
The Langmuir and Freundlich models were employed to fit the adsorption equilibrium data at various temperatures to help understand the interactions between the dyes and the HLDH. The forms of these models are expressed by Eqs 2 and 3, and the results are shown in Fig. 4 (Maneechakr & Karnjanakom, 2017).
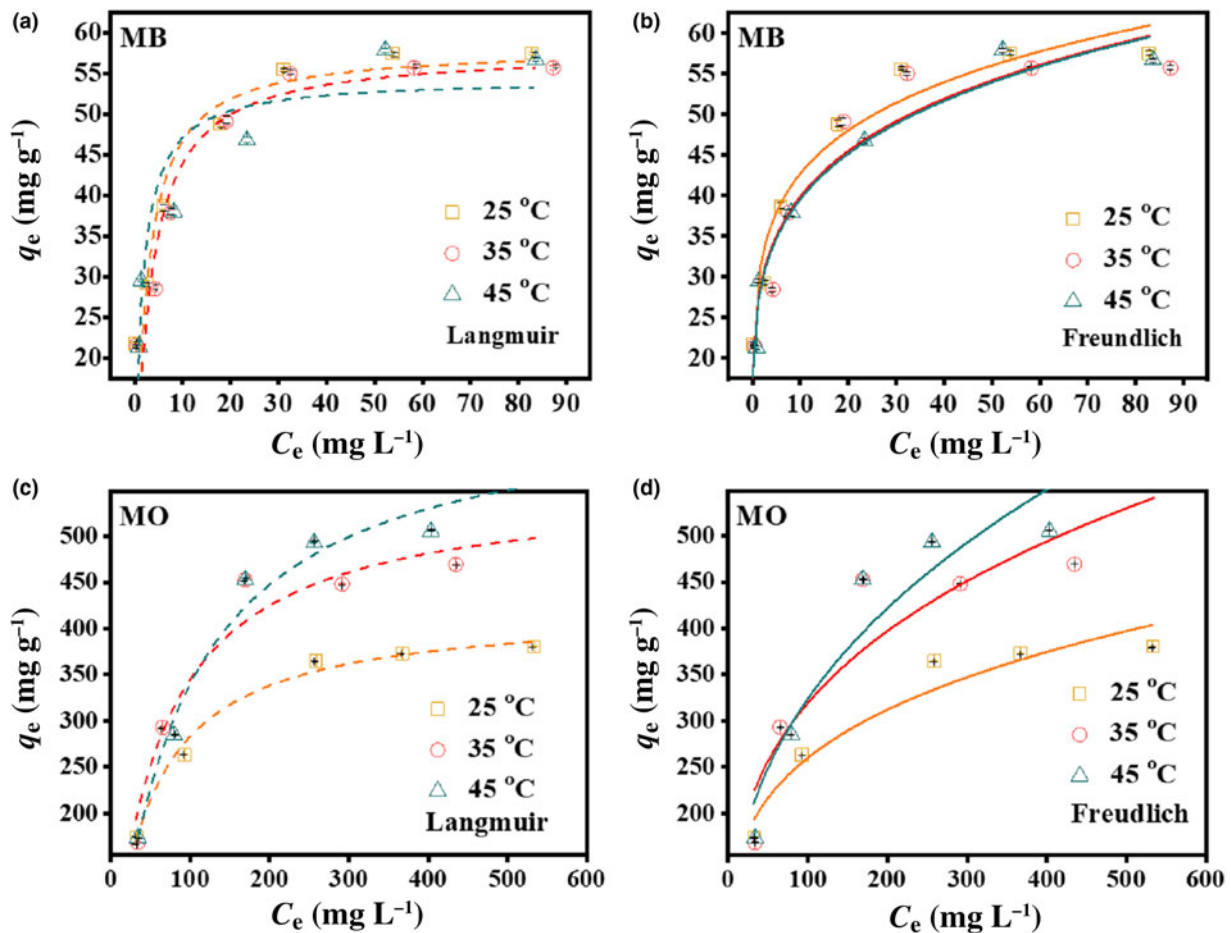
$$q_e = \frac{q_m K_L C_e}{1 + K_L C_e} \tag{2}$$

$$q_e = K_F C_e^{1/n} \tag{3}$$
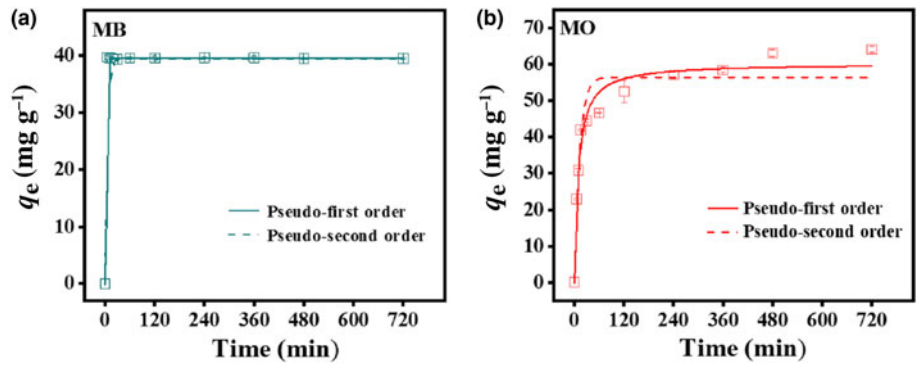
Fig. 2. Adsorption kinetics of (a) MB and (b) MO by the HLDH. Conditions: adsorbent dosage for MB/MO = 1 g L^{-1}; concentration of MB/MO = 100 mg L^{-1}; temperature = 25°C.

Fig. 3. Effect of pH on the absorption of (a) MB and (b) MO by HLDH. Conditions: adsorbent dosage for MB/MO = 1 g L^{-1}; concentration of MB/MO = 100 mg L^{-1}; temperature = 25°C.

Fig. 4. Adsorption isotherms of MB and MO on the HLDH using (a, c) Langmuir and (b, d) Freundlich models. Conditions: adsorbent for MB/MO = 1 g L^{-1}; contact time = 12 h; temperature = 25°C.

Table 3. Parameters fitted by the Langmuir and Freundlich models for MB and MO.

		MB			MO		
Isotherm model	Parameter	25°C	35°C	45°C	25°C	35°C	45°C
Langmuir	q_m	58.3	57.6	54.3	421.9	556.7	644.8
	K_L	0.42	0.32	0.64	0.02	0.02	0.01
	R^2	0.6874	0.7901	0.8819	0.9903	0.9525	0.9759
Freundlich	n	6.01	5.22	5.10	3.82	3.18	2.61
	K_F	29.11	25.56	25.08	78.10	75.23	55.23
	R^2	0.9562	0.9223	0.9623	0.9376	0.8446	0.9059

Table 4. Parameters fitted by the pseudo-first order and pseudo-second order kinetic models for MB and MO.

	Pseudo-first order			Pseudo-second order		
C_0 (mg L^{-1})	$q_{e,cal}$ (mg g^{-1})	k_1 (min^{-1})	R^2	$q_{e,cal}$ (mg g^{-1})	k_2 (min^{-1})	R^2
MB	0.5	0.0008	0.6174	39.7	0.1815	0.9999
MO	56.5	0.0805	0.9246	60.3	0.0018	0.9710

where q_e (mg g^{-1}) and C_e (mg L^{-1}) are the amounts of adsorption and the equilibrium concentration of MB or MO, respectively, K_L (L mg^{-1}) and q_m (mg g^{-1}) are the Langmuir constant and the maximum capacity of adsorption, respectively, and K_F (L mg^{-1}) and $1/n$ are Freundlich constants that relate to the adsorption amount and adsorption intensity, respectively. The relative parameter values extracted from the experimental data are listed in Table 3. By comparing the coefficients of determination (R^2), the Freundlich model was applicable for describing the removal of MB at all temperatures ($R_F^2 > R_L^2$), indicating that the multilayer adsorption occurred on the HLDH surface. In the case of MO, the Langmuir model better fitted the adsorption data, indicating a monolayer adsorption reaction for MO (Cui *et al.*, 2019).

Adsorption kinetics
The pseudo-first order (Eq. 4) and the pseudo-second order kinetic models (Eq. 5) were adopted to examine the adsorption mechanism (Hu & Han, 2019):

$$q_t = q_e(1 - e^{-k_1 t}) \qquad (4)$$

$$q_t = \frac{k_2 q_e^2 t}{1 + k_2 q_e t} \qquad (5)$$

where q_e and q_t (mg g^{-1}) are the amounts of dyes adsorbed on the HLDH at equilibrium and at time t (min), respectively, and k_1 (min^{-1}) and k_2 (g (mg min^{-1})$^{-1}$) represent the kinetic adsorption rate constants of the pseudo-first order and pseudo-second order models, respectively. The kinetic fitting results are shown in Fig. 2 and the parameters obtained are listed in Table 4. According to the R^2 values, the pseudo-second order kinetic model matched well with the adsorption of both dyes on the HLDH. Based on the assumption of a pseudo-second order kinetic model that chemical adsorption is the rate-limiting step of the adsorption process, it might be deduced that chemisorption was the main adsorption mechanism for both dyes (Guo *et al.*, 2018; Wang *et al.*, 2019).
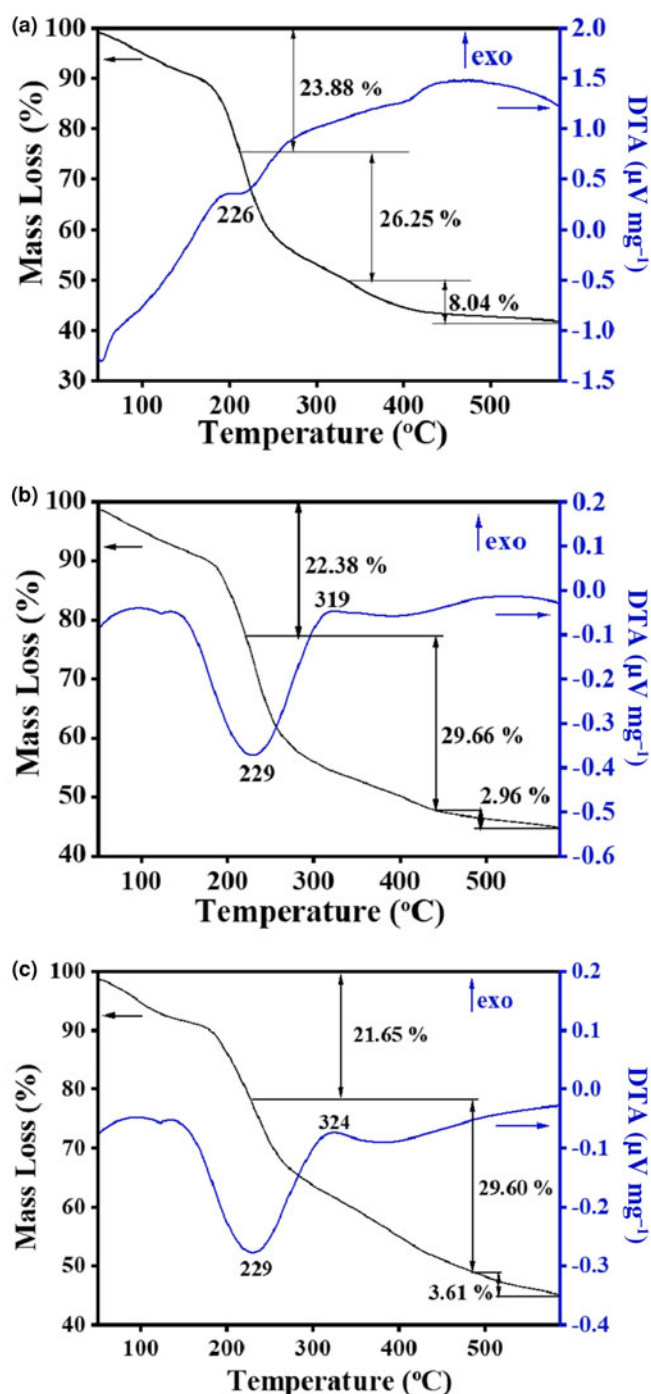
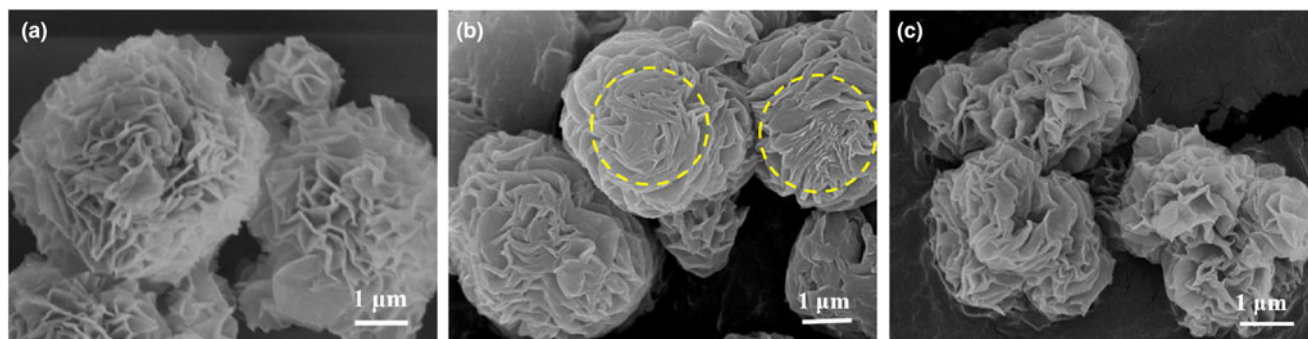**Fig. 5.** TG-DTA curves of (a) HLDH, (b) HLDH_MB and (c) HLDH_MO.

Fig. 6. SEM images of (a) HLDH, (b) HLDH_MB and (c) HLDH_MO.

Adsorption mechanism

The different removal mechanisms of MO and MB on the HLDH were elucidated comprehensively by characterization of the solid products after reaction. Three major mass-loss stages are observed in the TG-DTA curve of the HLDH (Fig. 5a). The first mass-loss event before 210°C (23.88%) corresponds to the loss of adsorbed water (Zhou *et al.*, 2010). The second mass-loss event at 210–335°C (26.25%) is attributed to the decomposition of the SDS molecules in the interlayer (Chen & Song, 2013). The third mass-loss event at 335–577°C (8.04%) is assigned to the dehydroxylation of the HLDH layers, indicating the collapse of the layered structure of the HLDH during this stage (Zhang *et al.*, 2019b). After reaction, similar mass-loss stages were observed for both HLDH_MB and HLDH_MO (Fig. 5b,c), except for the greater mass-loss ratio due to organic molecules at 229°C. This phenomenon might be caused by the anchored organic dyes on the HLDH, which increased the organic content. This was also observed in SEM (Fig. 6) with the occurrence of stacked nanoflakes after removal of the dyes, and with the bands attributed to MO and MB in the FTIR spectra (Fig. 7). In addition, compared with the FTIR spectra of pure HLDH, the O–H band of the HLDH in the HLDH_MB and HLDH_MO shifted from 3506 to 3455 and 3479 cm^{-1}, respectively. Previous studies have reported that a blue shift of the O–H band suggests electrostatic interaction (Shenvi *et al.*, 2015) or hydrogen bonding (Zhao *et al.*, 2015). Combined with the ζ-potential analysis (Fig. S1), electrostatic attraction should contribute to MB removal, whereas hydrogen bonding occurred in MO removal.

The XRD traces of the HLDH, HLDH_MB and HLDH_MO are shown in Fig. 8. In the HLDH, the (003), (006) and (009) peaks were observed at 3.28, 6.59 and 9.91°2θ, respectively. The corresponding d_{003} basal spacing was 2.72 nm, suggesting the existence of intercalated SDS in the interlayer (Dou *et al.*, 2015). After adsorption, the typical reflections of the LDH peaks were still visible, except for the shift of the (003) planes in the XRD traces of HLDH_MB and HLDH_MO (Fig. 8). In general, the shift of the (003) plane relates to the exchangeable ions in the interlayer (Deák *et al.*, 2018), suggesting that MO and MB entered the interlayer of the LDH. Notably, the *d*-value did not change after MB removal. As the chain length of MB (1.43 nm) is smaller than that of SDS (1.85 nm), we could infer that SDS and MB both existed in the interlayer, wherein MB could interact with SDS to form a monolayer (SDS-MB) *via* hydrophobic and electrostatic interaction (Milagres *et al.*, 2019). In the case of MO, the *d*-value decreased after adsorption, indicating that MO replaced SDS *via* anion exchange in the LDH interlayer because the length of MO (1.35 nm) is smaller than that of the SDS chain (Zhang *et al.*, 2019b).
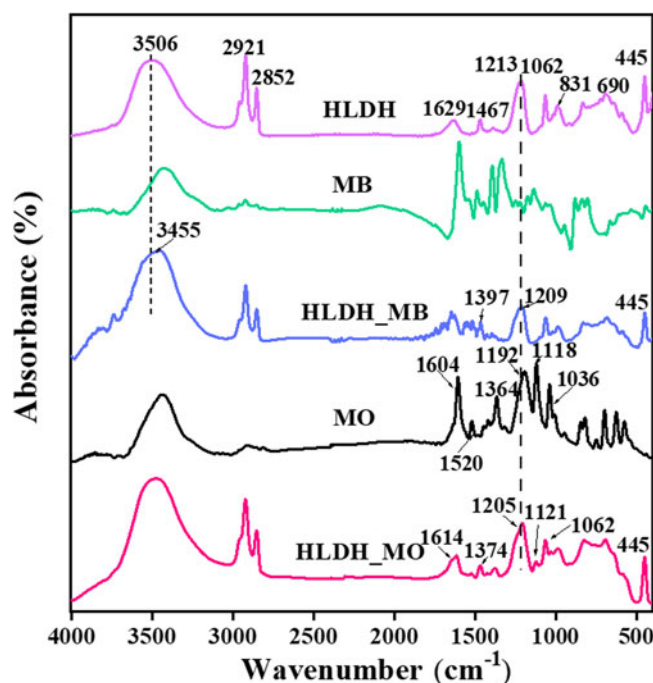

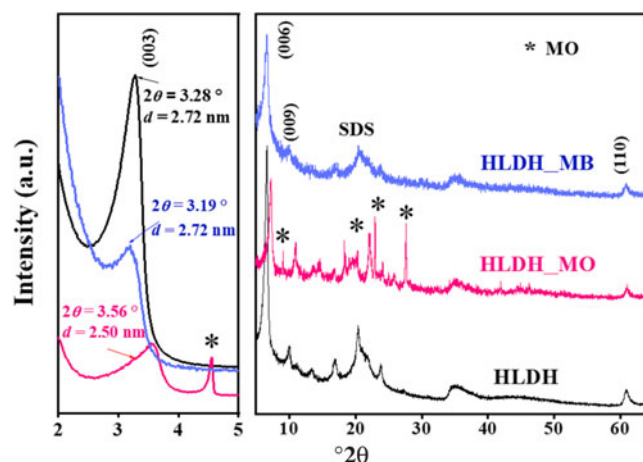**Fig. 7.** FTIR spectra of HLDH, HLDH_MB and HLDH_MO

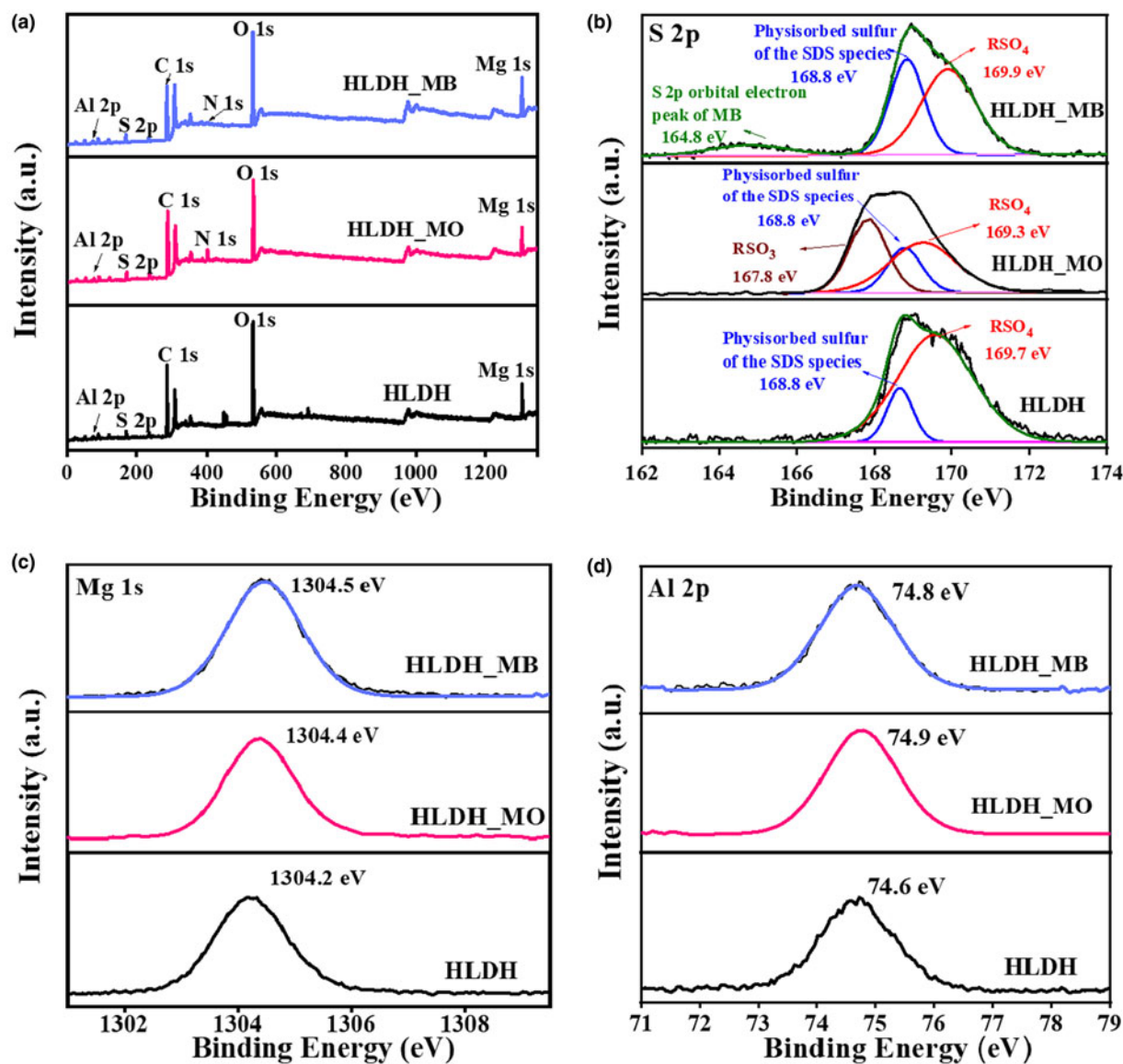**Fig. 8.** XRD traces of HLDH, HLDH_MB and HLDH_MO.

Fig. 9. XPS spectra of (a) wide scan, (b) S 2p, (c) Mg 1s and (d) Al 2p before and after removal of MB/MO on the HLDH.

The XPS analysis results of the solid products are presented in Fig. 9. After adsorption, the new N 1s peak belonging to MB and MO was observed in the XPS spectrum (Fig. 9a). As demonstrated by the S 2p spectra (Fig. 9b), the HLDH exhibited two peaks at 169.7 and 168.8 eV, which were assigned to the sulfate (RSO_4) and physiosorbed sulfur of SDS species, respectively (Madec *et al.*, 2014). After adsorption, an additional peak was observed at 164.8 eV, corresponding to the S 2p orbital electron peak of MB. The peak at 167.8 eV, ascribed to the RSO_3 of MO (Salazar *et al.*, 2016; Kumari *et al.*, 2020), is indicative of the successful capture of MB and MO on the HLDH. In addition, the binding energy of RSO_4 was shifted in the spectra of the HLDH_MO and HLDH_MB, revealing that the chemical environment of SDS had changed due to the adsorption of the dyes. Moreover, red shifts of Mg 1s (Fig. 9c) and Al 2p (Fig. 9d) were observed after the removal of both dyes, illustrating that the electrodensity of the host layer had changed (Sun *et al.*, 2021). Combined with the XRD and FTIR results, this phenomenon might be due to the fact that MO replaced SDS during anion exchange and then reacted with the host layer of the LDH *via* hydrogen bonding, while the cationic MB attached onto SDS *via* hydrophobic and electrostatic interactions, resulting in changes to the electrodensity.

Based on the above analyses, it is clear that SDS played vital role in the removal of anionic MO and cationic MB by the HLDH. The anionic MO replaced DS⁻ *via* anion exchange and was intercalated into the HLDH interlayer. However, the strong affinity between MB and DS⁻ led to the formation of a DS-MB monolayer, which promoted anchoring of MB on the HLDH, as is schematically depicted in Fig. 10.

Conclusions

Hierarchical HLDH intercalated with SDS *via* a soft-template mechanism exhibited superior removal performance regarding MO and MB dyes. The adsorption of MO (421.9–644.8 mg g⁻¹) was significantly higher than that of MB (58.3–54.3 mg g⁻¹). Temperature strongly influenced the adsorption behaviour of
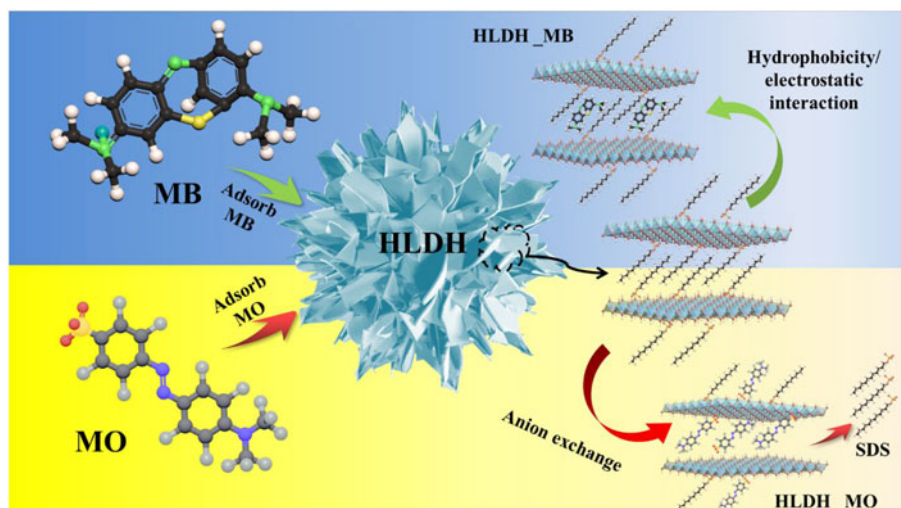
Fig. 10. Schematic illustration of MO and MB adsorption by the HLDH.

MO, while it had a negligible effect on MB removal, implying different removal pathways for MO and MB by the HLDH. The kinetic studies demonstrated that the removal of both dyes was controlled by chemisorption, and this is attributed mainly to the SDS; that is, MO replaced DS^- *via* anion exchange, whereas MB showed strong affinity to DS^- *via* hydrophobic and electrostatic interactions, and both were eventually intercalated into the interlayer of the LDH. This work provides a theoretical guideline for the removal of charged dyes using HLDH and deepens our understanding of the removal mechanism.

References

Abderrazek K., Uheida A., Seffen M., Muhammed M., Srasra N.F. & Srasra E. (2015) Photocatalytic degradation of indigo carmine using [Zn-Al] LDH supported on PAN nanofibres. *Clay Minerals*, **50**, 185–197.

Arif M., Liu G., Yousaf B., Ahmed R., Irshad S., Ashraf A. *et al.* (2021) Synthesis, characteristics and mechanistic insight into the clays and clay minerals–biochar surface interactions for contaminants removal – a review. *Journal of Cleaner Production*, **310**, 127548.

Bayram T., Bucak S. & Ozturk D. (2020) BR13 dye removal using sodium dodecyl sulfate modified montmorillonite: equilibrium, thermodynamic, kinetic and reusability studies. *Chemical Engineering and Processing – Process Intensification*, **158**, 108186.

Chen Y. & Song Y.F. (2013) Highly selective and efficient removal of Cr(VI) and Cu(II) by the chromotropic acid-intercalated Zn-Al layered double hydroxides. *Industrial & Engineering Chemistry Research*, **52**, 4436–4442.

Cui W., Zhang X., Pearce C.I., Chen Y., Zhang S., Liu W. *et al.* (2019) Cr(III) adsorption by cluster formation on boehmite nanoplates in highly alkaline solution. *Environmental Science and Technology*, **53**, 11043–11055.

Deák Á., Csapó E., Juhász Á., Dékány I. & Janovák L. (2018) Anti-ulcerant kynurenic acid molecules intercalated Mg/Al-layered double hydroxide and its release study. *Applied Clay Science*, **156**, 28–35.

de Castro G.F., Ferreira J.A., Eulálio D., de Souza S.J., Novais S.V., Novais R.F. *et al.* (2018) Layered double hydroxides: matrices for storage and source of boron for plant growth. *Clay Minerals*, **53**, 79–89.

Dou L., Fan T. & Zhang H. (2015) A novel 3D oxide nanosheet array catalyst derived from hierarchical structured array-like CoMgAl-LDH/graphene nanohybrid for highly efficient NO_x capture and catalytic soot combustion. *Catalysis Science & Technology*, **5**, 5153–5167.

Gao L., Sun J., Xu W. & Xiao G. (2016) Catalytic pyrolysis of natural algae over Mg-Al layered double oxides/ZSM-5 (MgAl-LDO/ZSM-5) for producing bio-oil with low nitrogen content. *Bioresource Technology*, **225**, 293–298.

Guo L., Xu Y., Zhuo M., Liu L., Xu Q., Wang L. *et al.* (2018) Highly efficient removal of Gd(III) using hybrid hydrosols of carbon nanotubes/graphene oxide in dialysis bags and synergistic enhancement effect. *Chemical Engineering Journal*, **348**, 535–545.

Hong Y., Zhou H., Xiong Z., Liu Y., Yao G. & Lai B. (2019) Heterogeneous activation of peroxymonosulfate by CoMgFe-LDO for degradation of carbamazepine: efficiency, mechanism and degradation pathways. *Chemical Engineering Journal*, **391**, 123604.

Hu Y. & Han R. (2019) Selective and efficient removal of anionic dyes from solution by zirconium(IV) hydroxide-coated magnetic materials. *Journal of Chemical & Engineering Data*, **64**, 791–799.

Hu H., Wageh S., Al-Ghamdi A.A., Yang S., Tian Z., Cheng B. & Ho W. (2020) NiFe-LDH nanosheet/carbon fiber nanocomposite with enhanced anionic dye adsorption performance. *Applied Surface Science*, **511**, 145570.

Igwegbe C.A., Mohmmadi L., Ahmadi S., Rahdar A., Khadkhodaiy D., Dehghani R. & Rahdar S. (2019) Modeling of adsorption of methylene blue dye on Ho-CaWO4 nanoparticles using response surface methodology (RSM) and artificial neural network (ANN) techniques. *MethodsX*, **6**, 1779–1797.

Jiehu C., Chunlei W., Ming Z., Jie Z., Li F., Xiuhong D. *et al.* (2020) 2D to 3D controllable synthesis of three Zn-Co-LDHs for rapid adsorption of MO by TEA-assisted hydrothermal method. *Applied Surface Science*, **534**, 147564.

Jing C., Zhu Y., Liu X., Ma X., Dong F., Dong B. *et al.* (2019) Morphology and crystallinity-controlled synthesis of etched CoAl LDO/MnO2 hybrid nanoarrays towards high performance supercapacitors. *Journal of Alloys and Compounds*, **806**, 917–925.

Kumari S., Khan A.A., Chowdhury A., Bhakta A.K., Mekhalif Z. & Hussain S. (2020) Efficient and highly selective adsorption of cationic dyes and removal of ciprofloxacin antibiotic by surface modified nickel sulfide nanomaterials: kinetics, isotherm and adsorption mechanism. *Colloids and Surfaces A: Physicochemical and Engineering Aspects*, **586**, 124264.

Li B. & He J. (2008) Multiple effects of dodecanesulfonate in the crystal growth control and morphosynthesis of layered double hydroxides. *Journal of Physical Chemistry C*, **112**, 10909–10917.

Lin S.-T., Tran H.N., Chao H.-P. & Lee J.-F. (2018) Layered double hydroxides intercalated with sulfur-containing organic solutes for efficient removal of cationic and oxyanionic metal ions. *Applied Clay Science*, **162**, 443–453.

Liu Y., Yu Z., Wang Q., Zhu X., Long R. & Li X. (2021) Application of sodium dodecyl sulfate intercalated Co-Al LDH composite materials (RGO/PDA/ SDS-LDH) in membrane separation. *Applied Clay Science*, **209**, 106138.

Lu L., Li J., Ng D.H.L., Yang P., Song P. & Zuo M. (2017) Synthesis of novel hierarchically porous Fe_3O_4@MgAl–LDH magnetic microspheres and its superb adsorption properties of dye from water. *Journal of Industrial and Engineering Chemistry*, **46**, 315–323.

Ma L., Wang Q., Islam S.M., Liu Y., Ma S. & Kanatzidis M.G. (2016) Highly selective and efficient removal of heavy metals by layered double hydroxide intercalated with the MoS_4^{2-} ion. *Journal of the American Chemical Society*, **138**, 2858–2866.

Madec L., Xia J., Petibon R., Nelson K.J., Sun J.-P., Hill I.G. & Dahn J.R. (2014) Effect of sulfate electrolyte additives on $LiNi_{1/3}Mn_{1/3}Co_{1/3}O_2$/graphite pouch cell lifetime: correlation between XPS surface studies and electrochemical test results. *Journal of Physical Chemistry C*, **118**, 29608–29622.

Maneechakr P. & Karnjanakom S. (2017) Adsorption behaviour of Fe(II) and Cr (VI) on activated carbon: surface chemistry, isotherm, kinetic and thermodynamic studies. *Journal of Chemical Thermodynamics*, **106**, 104–112.

Miao J., Zhao X., Zhang Y.-X., Lei Z.-L. & Liu Z.-H. (2021) Preparation of hollow hierarchical porous CoMgAl-borate LDH ball-flower and its calcinated product with extraordinary adsorption for Congo red and methyl orange. *Applied Clay Science*, **207**, 106093.

Milagres J.L., Bellato C.R., Ferreira S.O., Guimarães L.M., Tonon G.J.P. & Bolandini A. (2019) Simultaneous removal process of divalent metal and anionic and cationic dyes by layered reconstruction with hydrocalumite intercalated with dodecyl sulfate. *Colloids and Surfaces A: Physicochemical and Engineering Aspects*, **582**, 123890.

Romero Ortiz G., Lartundo-Rojas L., Samaniego-Benitez J.E., Jimenez-Flores Y., Calderon H.A. & Mantilla A. (2021) Photocatalytic behavior for the phenol degradation of ZnAl layered double hydroxide functionalized with SDS. *Journal of Environmental Management*, **277**, 111399.

Salazar C., Lach J., Ruckerl F., Baumann D., Schimmel S., Knupfer M. *et al.* (2016) Stm study of Au(111) surface-grafted paramagnetic macrocyclic complexes [Ni2L(Hmba)](+) *via* ambidentate coligands. *Langmuir*, **32**, 4464–4471.

Shan R.-r., Yan L.-g., Yang K., Yu S.-j., Hao Y.-f., Yu H.-q. & Du B. (2014) Magnetic Fe_3O_4/MgAl-LDH composite for effective removal of three red dyes from aqueous solution. *Chemical Engineering Journal*, **252**, 38–46.

Shenvi S.S., Isloor A.M., Ismail A.F., Shilton S.J. & Al Ahmed A. (2015) Humic acid based biopolymeric membrane for effective removal of methylene blue and rhodamine B. *Industrial & Engineering Chemistry Research*, **54**, 4965–4975.

Suh M.J., Weon S., Li R., Wang P. & Kim J.H. (2020) Enhanced pollutant adsorption and regeneration of layered double hydroxide-based photoregenerable adsorbent. *Environmental Science & Technology*, **54**, 9106–9115.

Sun Y., Zhou J., Cai W., Zhao R. & Yuan J. (2015) Hierarchically porous NiAl-LDH nanoparticles as highly efficient adsorbent for p-nitrophenol from water. *Applied Surface Science*, **349**, 897–903.

Sun H., Zhang W., Li J.-G., Li Z., Ao X., Xue K.-H. *et al.* (2021) Rh-engineered ultrathin NiFe-LDH nanosheets enable highly-efficient overall water splitting and urea electrolysis. *Applied Catalysis B: Environmental*, **284**, 119740.

Wang L., Song H., Yuan L., Li Z., Zhang P., Gibson J.K. *et al.* (2019) Effective removal of anionic Re(VII) by surface-modified Ti_2Ct_xMXene nanocomposites: implications for Tc(VII) sequestration. *Environmental Science & Technology*, **53**, 3739–3747.

Weber C., Heuser M., Mertens G. & Stanjek H. (2014) Determination of clay mineral aspect ratios from conductometric titrations. *Clay Minerals*, **49**, 17–26.

Xu Z.P., Jin Y., Liu S., Hao Z.P. & Lu G.Q. (2008) Surface charging of layered double hydroxides during dynamic interactions of anions at the interfaces. *Journal of Colloid and Interface Science*, **326**, 522–529.

Yang D.-S., Wang M.-K. & Wang S.-L. (2004) Synthesis of Li/Al layered double hydroxide-guest composites under mild acid conditions. *Clay Minerals*, **39**, 115–121.

Yuan W., Zhang L., Liu Y., Fu P., Huang Y., Wang L. *et al.* (2020) Sulfide removal and water recovery from ethylene plant spent caustic by suspension crystallization and its optimization *via* response surface methodology. *Journal of Cleaner Production*, **242**, 118439.

Zhang P., He T., Li P., Zeng X. & Huang Y. (2019a) New insight into the hierarchical microsphere evolution of organic three-dimensional layer double hydroxide: the key role of the surfactant template. *Langmuir*, **35**, 13562–13569.

Zhang P., Ouyang S., Li P., Huang Y. & Frost R.L. (2019b) Enhanced removal of ionic dyes by hierarchical organic three-dimensional layered double hydroxide prepared *via* soft-template synthesis with mechanism study. *Chemical Engineering Journal*, **360**, 1137–1149.

Zhao F., Repo E., Yin D., Meng Y., Jafari S. & Sillanpaa M. (2015) EDTA-cross-linked beta-cyclodextrin: an environmentally friendly bifunctional adsorbent for simultaneous adsorption of metals and cationic dyes. *Environmental Science and Technology*, **49**, 10570–10580.

Zheng Y., Cheng B., You W., Yu J. & Ho W. (2019) 3D hierarchical graphene oxide–NiFe LDH composite with enhanced adsorption affinity to Congo red, methyl orange and Cr(VI) ions. *Journal of Hazardous Materials*, **369**, 214–225.

Zhou J.Z., Wu Y.Y., Liu C., Orpe A., Liu Q., Xu Z.P. *et al.* (2010) Effective self-purification of polynary metal electroplating wastewaters through formation of layered double hydroxides. *Environmental Science & Technology*, **44**, 8884–8890.